

# The long-term evolution of neutron star merger remnants – I. The impact of r-process nucleosynthesis

S. Rosswog<sup>1\*</sup>, O. Korobkin<sup>1</sup>, A. Arcones<sup>2,3</sup>, F.-K. Thielemann<sup>4</sup>, T. Piran<sup>5</sup>

<sup>1</sup>*The Oskar Klein Centre, Department of Astronomy, AlbaNova, Stockholm University, SE-106 91 Stockholm, Sweden*

<sup>2</sup>*Institut für Kernphysik, Technische Universität Darmstadt, 64289 Darmstadt, Germany*

<sup>3</sup>*GSI Helmholtzzentrum für Schwerionenforschung, Planckstr. 1, 64291 Darmstadt, Germany*

<sup>4</sup>*Department of Physics, University of Basel, Klingelbergstrasse 82, CH-4056 Basel, Switzerland*

<sup>5</sup>*Racah Institute of Physics, The Hebrew University, Jerusalem 91904, Israel*

Accepted 2013. Received 2013; in original form 2013

## ABSTRACT

We follow the longterm evolution of the dynamic ejecta of neutron star mergers for up to 100 years and over a density range of roughly 40 orders of magnitude. We include the nuclear energy input from the freshly synthesized, radioactively decaying nuclei in our simulations and study its effects on the remnant dynamics. Although the nuclear heating substantially alters the longterm evolution, we find that running nuclear networks over purely hydrodynamic simulations (i.e. without heating) yields actually acceptable nucleosynthesis results. The main dynamic effect of the radioactive heating is to quickly smooth out inhomogeneities in the initial mass distribution, subsequently the evolution proceeds self-similarly and after 100 years the remnant still carries the memory of the initial binary mass ratio. We also explore the nucleosynthetic yields for two mass ejection channels. The dynamic ejecta very robustly produce ‘strong’ r-process elements with  $A > 130$  with a pattern that is essentially independent of the details of the merging system. From a simple model we find that neutrino-driven winds yield ‘weak’ r-process contributions with  $50 < A < 130$  whose abundance patterns vary substantially between different merger cases. This is because their electron fraction, set by the ratio of neutrino luminosities, varies considerably from case to case. Such winds do not produce any  $^{56}\text{Ni}$ , but a range of radioactive isotopes that are long-lived enough to produce a second, radioactively powered electromagnetic transient in addition to the ‘macronova’ from the dynamic ejecta. While our wind model is very simple, it nevertheless demonstrates the potential of such neutrino-driven winds for electromagnetic transients and it motivates further, more detailed neutrino-hydrodynamic studies. The properties of the mentioned transients are discussed in more detail in a companion paper.

**Key words:** nuclear reactions, nucleosynthesis, abundances, transients, gamma-ray bursts

## 1 INTRODUCTION

The importance of compact binary mergers as sources of gravitational waves (GW; e.g. Cutler & Flanagan 1994; Maggiore 2007) and as central engines of short Gamma-ray bursts (Eichler et al. 1989; Narayan et al. 1991; Piran 2004; Nakar 2007; Lee & Ramirez-Ruiz 2007) has been appreciated for decades. Maybe more surprising is the fact that compact binary mergers have only been considered *seriously* as a possible production site of rapid neutron cap-

ture (‘r-process’) elements in roughly the last decade. This is particularly astonishing since there is general agreement that the final fate after their inspiral is a violent event in an extremely neutron-rich environment, exactly what is recognized to be needed as a cauldron to forge r-process elements. Moreover, Lattimer & Schramm (1974) had pointed out this possibility and they discussed its impact on cosmic nucleosynthesis even before the first binary neutron star had been discovered. In Lattimer et al. (1977) r-process nucleosynthesis is discussed in the context of a cold decompression of neutron star matter. In the last decade a number of studies found core-collapse supernovae to be seriously chal-

\* E-mail: Stephan.Rosswog@astro.su.se

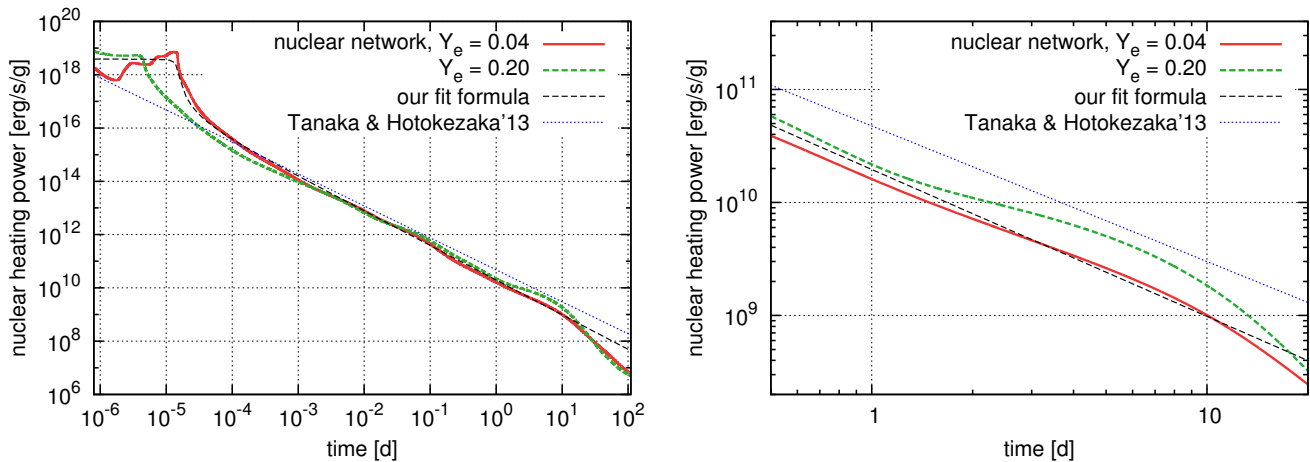


**Figure 1.** A comparison of the nuclear heating rates used in different approaches on different time-scales. The left panel depicts the whole duration of the event while the right panel focuses on a time scale of a few days, which is most relevant for the macronovae emission. The solid (red) and dashed (green) lines display heating rates for initial  $Y_e = 0.04$  (the typical value that results from initial beta-equilibrium plus subsequent electron/positron captures in our simulations) and  $Y_e = 0.2$  (the value adopted for dynamical ejecta in Barnes & Kasen (2013), based on the work of Roberts et al. (2011)). Also displayed is our analytic fit from Korobkin et al. (2012) and the one used in Tanaka & Hotokezaka (2013). For proper comparison, we have set the heating efficiency parameter  $\epsilon_{\text{th}} = 1$ . Note that the increased  $Y_e$  value results in a substantially larger heating rate in the epoch that is most relevant for macronovae.

lenged in providing suitable conditions to produce heavy r-process elements (e.g. Arcones et al. 2007; Fischer et al. 2010; Hüdepohl et al. 2010; Roberts et al. 2010)<sup>1</sup>. In parallel, several studies found that a robust r-process occurs in the dynamic ejecta of neutron star mergers (Freiburghaus et al. 1999; Goriely et al. 2011a; Roberts et al. 2011; Korobkin et al. 2012). These developments have changed the general perceptions and nowadays, neutron stars are accepted at least as serious contenders of core-collapse supernovae if not even *the* major candidate sites for the production of the heaviest, ‘strong r-process’ elements ( $A \gtrsim 130$ ). Even if the latter is true, at least one but probably more r-process sites must exist in addition. The dynamic ejecta of neutron star mergers are probably not a source of ‘weak r-process’ (Snedden et al. 2008), but the neutrino-driven winds that emerge in the aftermath of a merger (Dessart et al. 2009) could plausibly contribute to this r-process component. A third process by which neutron-rich matter may be shed in substantial amounts is the final disintegration of an accretion disc that occurs after many viscous time-scales ( $\sim$  seconds) when viscous dissipation and the recombination of nucleons into light nuclei conspire to unbind a substantial fraction of whatever is left from the disc at that time (Lee & Ramirez-Ruiz 2007; Beloborodov 2008; Metzger et al. 2008, 2009; Lee et al. 2009). Recent work (Fernández & Metzger 2013) suggests that  $\sim 10^{-2} M_{\odot}$  become unbound with  $Y_e \sim 0.2$ , in addition to the dynamic ejecta and the wind material. Nucleosynthesis features of such disc ejecta (partially also invoking neutrino flavour oscillations) have been studied by Surman et al. (2008), Caballero et al. (2012), Wanaajo & Janka (2012) and Malkus et al. (2012).

The astrophysical relevance of the dynamic ejecta from com-

pact binary mergers, however, goes beyond their roles as promising nucleosynthesis site. They are believed to also trigger short-lived electromagnetic transients powered by radioactivity, so-called ‘macronovae’ (Li & Paczyński 1998; Kulkarni 2005; Rosswog 2005; Metzger et al. 2010; Roberts et al. 2011; Goriely et al. 2011a; Metzger & Berger 2012; Kelley et al. 2012; Rosswog et al. 2013; Piran et al. 2013; Barnes & Kasen 2013). As we will discuss below, also the neutrino-driven winds may actually produce radioactively powered transients, though with different nuclear and electromagnetic properties than those from the dynamic ejecta. Both the LIGO and Virgo GW detectors are currently being upgraded (Abbott et al. 2009; Smith 2009; Sengupta et al. 2010) to a more than 10 times better sensitivity than the original versions of the instruments. This will increase the volume of accessible astrophysical sources by more than a factor of 1000 reaching a detection horizon of a few hundred Mpc for nsns mergers and about a Gpc for nsbh mergers (Abadie et al. 2010). Since the first events are expected to be around or even below threshold, accompanying electromagnetic signatures, such as r-process powered macronovae, could substantially boost the confidence in such a marginal detection (Nissanke et al. 2013; Kasliwal & Nissanke 2013). The heating from the nuclear decay may also suspend fallback accretion (Metzger et al. 2010) and thus cause a gap between prompt and late-time activity in short GRBs. Months after the merger, the dynamic ejecta may trigger radio flares when they dissipate their kinetic energies in the ambient medium (Nakar & Piran 2011; Piran et al. 2013) and this could possibly provide lower limits on the merger rates even before the GW detectors are fully operational.

In this paper we present a new study of neutron star merger ejecta that goes beyond previous work in several ways. First, rather than performing hydrodynamic simulations for  $\sim 20$  ms and then extrapolating the thermodynamic ejecta histories to  $\sim 10$  s (Freiburghaus et al. 1999; Goriely et al. 2011a; Roberts et al. 2011; Korobkin et al. 2012), our simulations

<sup>1</sup> A possible exception may be stars with the particular, and probably rare, combination of fast rotation and very large pre-collapse magnetic field (Winteler et al. 2012).

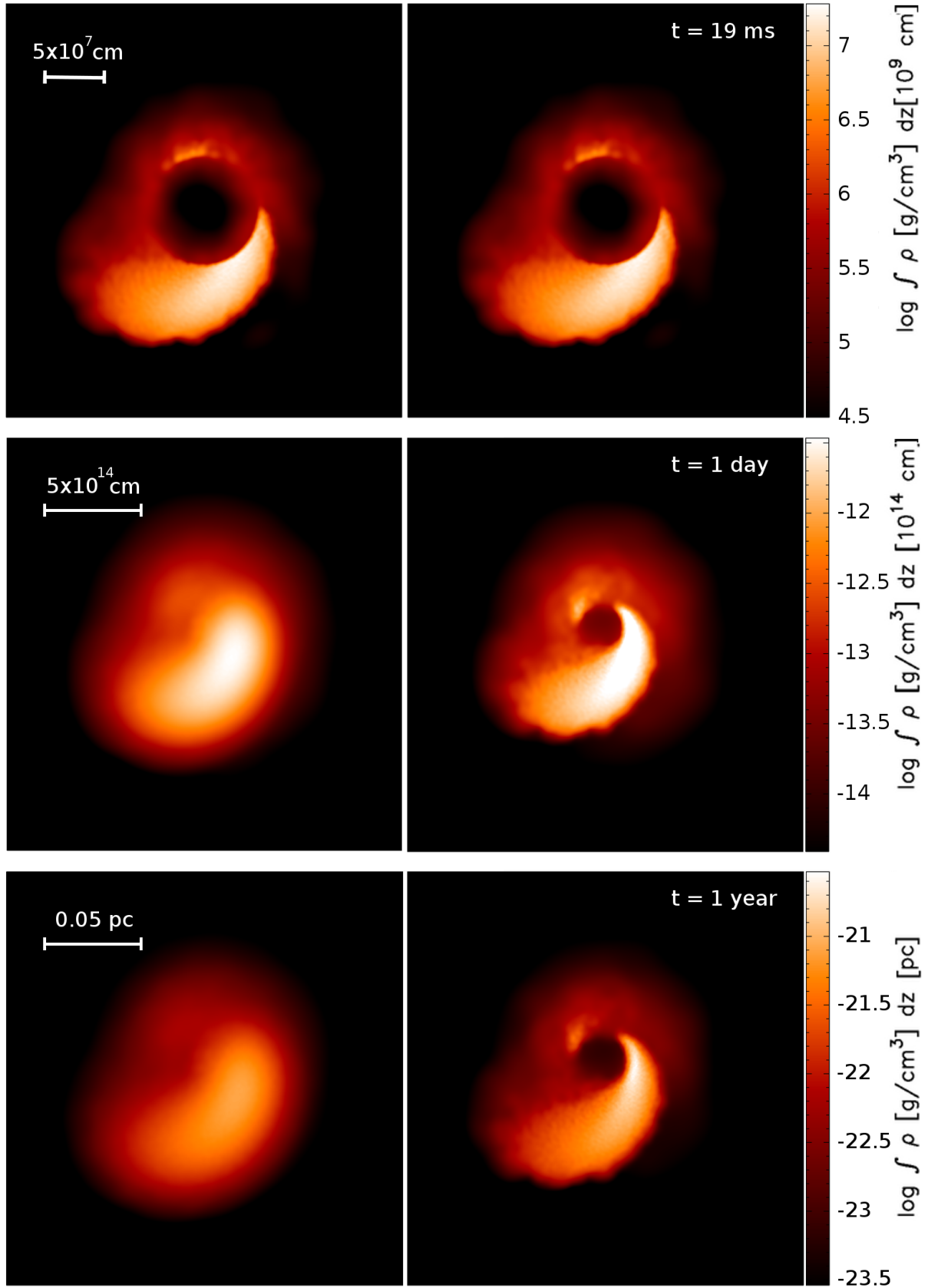


**Figure 2.** Illustration of the effect of radioactive heating on the remnant evolution (for run B, see Tab. 1;  $1.3$  and  $1.4 M_{\odot}$ ). The evolution including the effects from radioactive decays is shown in the left column, and the one without in the right column. The first row shows the initial configuration (corresponding to  $t = 19$  ms of our original merger simulation; in the spherical central region matter has been cut out and has been replaced by a point mass). The second row corresponds to the matter configuration after  $t = 1$  d, roughly when the resulting ‘macronova’ will reach its peak bolometric luminosity. The last row shows the remnant structure at  $t = 1$  year.

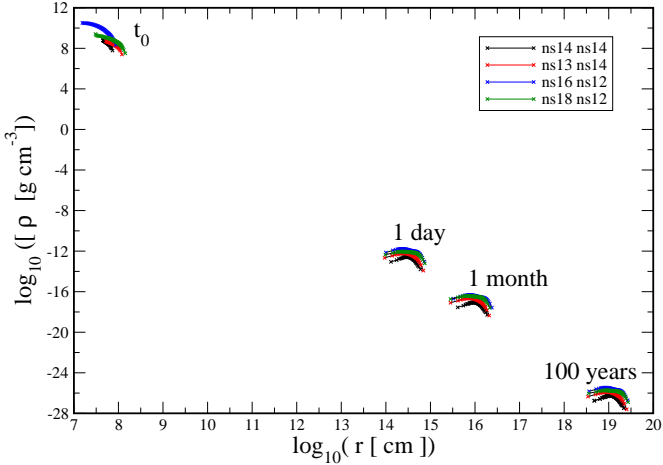


**Figure 3.** Density distribution (50 bins for each case) inside the remnants at chosen snapshots. For each time label, the closest available data set was used. Depending on the exact merger environment, the late-time evolution may be impacted by ambient medium effects.

directly follow the hydrodynamic evolution of the ejecta for time-scales as long as 100 years after the merger. We stop our simulations at this point since, by this time, the ejecta likely have swept up an amount of mass from the ambient medium that is comparable to their own mass and so they start to slow down. Where and when exactly this will happen depends sensitively on the environment in which the merger occurs. This, in turn, depends on the kick velocity and the inspiral time of the particular binary system. The ejecta from mergers that occur in the galactic plane may be braked much earlier than those of mergers occurring a few kpc outside of their host galaxies, see the estimates below. Secondly, all existing studies have assumed that the energetic feedback from nuclear reactions on the hydrodynamic evolution can be neglected, and that it is safe to just post-process given trajectories for nucleosynthesis. The standard approach is to ignore nuclear energy release in the hydrodynamics part of the calculation, subsequently run nuclear networks along given density trajectories and finally to reconstruct the temperature histories from the entropy that was generated in nuclear reactions (Freiburghaus et al. 1999). In other words, it is usually assumed that the nuclear energy input does not substantially impact on the density evolution. Analytic one-zone models (Goriely et al. 2011b) seem to support this assumption, but as we will show below, the nuclear feedback has indeed a serious impact on the longterm evolution of neutron star merger remnants. Nevertheless, on the short time-scales on which the r-process occurs ( $\sim$  seconds) its impact is still small enough so that post-processing hydrodynamic trajectories is an admissible procedure which yields acceptable nucleosynthesis results.

Third, we are able to follow the ejecta through the times when radioactively powered transients should peak ( $\sim$  days) and up to the point when the radio flares from the interaction with the ambient medium are expected ( $\sim$  years). The

available geometric information allows us to abandon the assumption of spherical symmetry that was adopted in all previous calculations of ‘macronovae’ light curves. This complements recent approaches by Barnes & Kasen (2013) and Kasen et al. (2013) who use sophisticated radiative transfer, but make strongly simplifying assumptions about the ejecta geometry. These results are discussed in a companion paper (Grossman et al. 2013), subsequently referred to as ‘Paper II’.

This paper is structured as follows. In Sec. 2 we briefly summarize our simulations and in Sec. 3 we discuss the remnant structure and its close-to-homologous evolution during the first century after the merger where we pay particular attention to the effects of radioactive heating. In Sec. 4 the nucleosynthesis from both dynamic ejecta and neutrino-driven winds is discussed, the corresponding radioactively powered electromagnetic signals are examined in detail in Paper II. We summarize our results in Sec. 5.

## 2 SIMULATIONS

### 2.1 When to stop?

In our simulations we follow the ejecta of neutron star mergers as they expand into vacuum. In Nature, a merger is engulfed by an external, though dilute medium of a density  $\rho_{\text{amb}} = m_p n_{\text{amb}}$  that depends on the actual merger location. Mergers that occur early after the neutron star binaries have formed take place close to the midplane of their host galaxies where the density may be  $n \sim 1 \text{ cm}^{-3}$ . On the other hand, binary systems that had time to travel a few kpc out of the midplane (Narayan et al. 1992; Fryer et al. 1999; Bloom et al. 2002; Rosswog et al. 2003; Fong et al. 2010) may occur in a much lower density surrounding. The initial expansion stages will be unaffected by the ambient medium, but once the swept up amount of matter is comparable to the ejected mass,  $m_{\text{su}} \approx m_{\text{ej}}$ , the ejecta start to slow down. This transition defines the deceleration radius of

$$R_{\text{dec}} = 0.5 \text{ pc} \left( \frac{m_{\text{ej}}}{10^{-2} M_{\odot}} \frac{1 \text{ cm}^{-1/3}}{n_{\text{amb}}} \right)^{1/3}, \quad (1)$$

which is reached after the deceleration time

$$\tau_{\text{dec}} = 15 \text{ yr} \left( \frac{m_{\text{ej}}}{10^{-2} M_{\odot}} \frac{1 \text{ cm}^{-1/3}}{n_{\text{amb}}} \right)^{1/3} \left( \frac{0.1 c}{v_{\text{ej}}} \right). \quad (2)$$

Both estimates are rather insensitive to the poorly known ambient matter density. Thus, ambient matter effects start to become noticeable after 15 (150) years in an environment of  $n = 1(10^{-3}) \text{ cm}^{-3}$ . Since the effects from an ambient medium are not taken into account in our study, we stop the simulations 100 years after the coalescence.

### 2.2 Hydrodynamic simulations

Typically neutron star merger simulations are only performed up to  $\sim 20$  ms, mainly because of serious time-step restrictions due to the Courant–Friedrichs–Lewy stability criterion. The simulations that are presented here, in contrast, are performed up to 100 years after the coalescence. Therefore, we have information on the remnant geometry throughout the phases where the major electromagnetic emission – from radioactivity in the neutrino-driven

**Table 1.** Overview over the performed simulations:  $m_1$  and  $m_2$  are masses of the neutron stars,  $N_{\text{SPH}}$  is the number of SPH particles and  $t_{\text{end}}$  is the final simulation time. Properties of the dynamical ejecta include their mass  $m_{\text{ej}}$ , kinetic energy  $E_{\text{kin}}$  and thermalized nuclear energy  $E_{\text{nuc}}$ . Neutrino-related quantities:  $L_{\nu_e}$  and  $L_{\bar{\nu}_e}$  are neutrino and anti-neutrino luminosities,  $\langle E \rangle_{\nu_e}$  and  $\langle E \rangle_{\bar{\nu}_e}$  are the average neutrino energies, and  $Y_e^{\text{fin,wind}}$  is the estimated asymptotic  $Y_e$  in the neutrino driven wind (Qian et al. 1997).

Run	$m_1$	$m_2$	$N_{\text{SPH}}$	$t_{\text{end}}$	$m_{\text{ej}}$	$E_{\text{kin}}$	$E_{\text{nuc}}$	$L_{\nu_e}$	$L_{\bar{\nu}_e}$	$\langle E \rangle_{\nu_e}$	$\langle E \rangle_{\bar{\nu}_e}$	$Y_e^{\text{fin,wind}}$
	( $M_{\odot}$ )	( $M_{\odot}$ )	( $10^6$ )	(ms)	( $10^{-2}M_{\odot}$ )	( $10^{50}$ erg)		( $10^{52}$ erg/s)		(MeV)	(MeV)	(MeV)
A	1.4	1.4	1.0	13.4	1.3	2.6	0.8	3.0	6.1	7.8	14.3	0.28
B	1.3	1.4	2.7	20.3	1.4	2.4	0.9	3.1	6.0	8.0	14.4	0.30
C	1.6	1.2	1.0	14.8	3.3	6.8	2.1	7.0	11.0	9.5	15.0	0.36
D	1.8	1.2	1.0	21.4	3.4	7.5	2.2	5.0	7.2	9.4	13.6	0.40

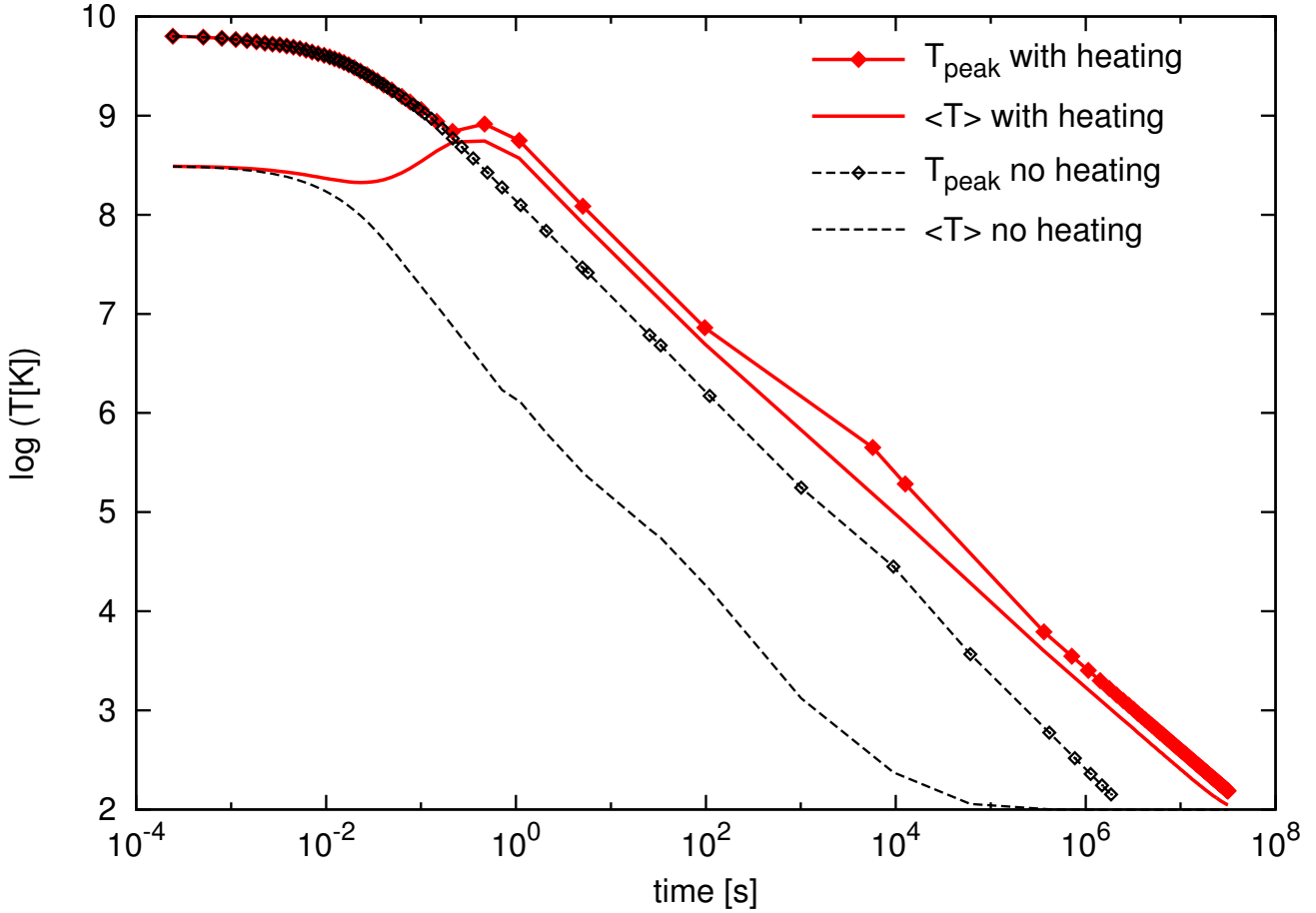


**Figure 4.** Illustration of the effect of radioactive heating on the temperature evolution (for run B, see Tab. 1; 1.3 and 1.4  $M_{\odot}$ ). The peak temperature with diamond symbol, and the average with a solid line; for comparison the values without heating are shown in black.

winds and dynamic ejecta and the interaction with ambient material– is expected.

The simulations of this paper start from the final matter distributions of the runs presented in Rosswog et al. (2013) and Rosswog (2013). These simulations were performed with a 3D, Smooth Particle Hydrodynamics (SPH) code whose implementation details have been described in the literature (Rosswog et al. 2000; Rosswog & Davies 2002; Rosswog & Liebendörfer 2003; Rosswog & Price 2007). For a general overview over the SPH method, see, for example, the recent

reviews of Monaghan (2005), Rosswog (2009) and Springel (2010).

The code that we use for the subsequent longterm evolution of the ejecta is a variant of the above described SPH code, but with different units and physics ingredients (Rosswog et al. 2008). Since the ejecta densities change in the first  $\sim 100$  years by as many as  $\sim 40$  orders of magnitude (!) special attention has to be paid to the equation of state (EOS). The initial merger simulations make use of the Shen-EOS (Shen et al. 1998a,b), the longterm evolution is followed us-

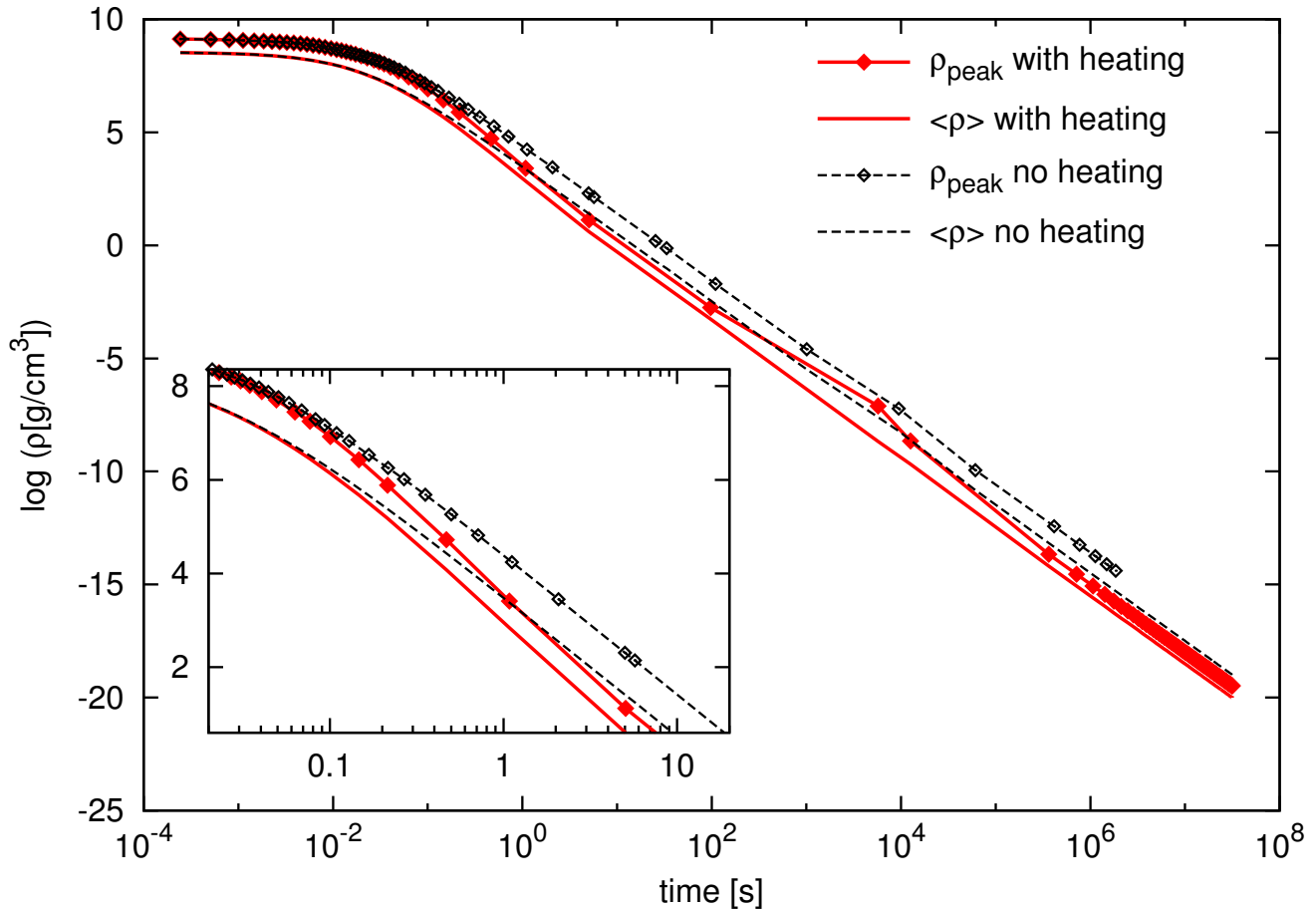


**Figure 5.** Illustration of the effect of radioactive heating on the density evolution (for run B, see Tab. 1; 1.3 and 1.4  $M_{\odot}$ ). The labelling of the curves is as in the previous figures. Inset zooms on the density evolutions for the period around  $t \sim 1$  s, when heating has maximal impact on the density, decreasing it by about one order of magnitude.

ing the Helmholtz EOS (Timmes & Swesty 2000) which is the state-of-the-art for matter at roughly white dwarf densities. It uses in particular a completely general electron EOS which is recovered via a sophisticated interpolation scheme from pre-calculated tables. When the density and temperature drop during the matter expansion to values near the lower limits of the Helmholtz EOS, we smoothly switch over to a Maxwell–Boltzmann gas plus radiation.

Our main interest here is the long-term evolution of the dynamically ejected matter. As stated above, this material cannot be evolved for long time-scales together with the dense inner parts of the remnant since the high sound speed near nuclear matter density ( $\sim 0.3 c$ ) enforces prohibitively small numerical time-steps. Therefore, we replace the inner part of the remnant at the end of the initial simulation ( $\sim 18$  ms) by a point mass. This inner part is defined by a radius that safely includes all matter with close to zero and negative radial velocity, typically this radius is  $R_{\text{cut}} = 300$  km. Apart from reducing the SPH particle number, this configuration now allows for much larger (and increasing!) numerical time-steps which make this long-term simulation feasible in the first place.

We follow the evolution of the ejecta including the radioactive heating for a number of exemplary systems: a) an

equal mass merger with  $2 \times 1.4 M_{\odot}$ , b) a merger with a slight asymmetry, 1.4 and 1.3  $M_{\odot}$ , c) a merger of a 1.6-1.2  $M_{\odot}$  system and finally d) the merger of a 1.8  $M_{\odot}$  ns with a 1.2  $M_{\odot}$  ns (see Tab. 1). For all systems the simulations stop 100 years after the merger.

For the involved nucleosynthesis calculations we make use of the nuclear reaction network of Winteler (Winteler 2012; Winteler et al. 2012) which represents an update of the Bas-Net network (Thielemann et al. 2011).

### 2.3 Implementation of the r-process heating

During the hydrodynamical evolution we include the heating due to radioactive decays. We had recently explored the nucleosynthesis in neutron star merger ejecta (Korobkin et al. 2012) and found that, in agreement with the findings of other groups (Metzger et al. 2010; Roberts et al. 2011; Goriely et al. 2011a), the heating history is rather insensitive to details of both the merging system and the individual matter trajectory can be well-fit as a function of time. In the current study, we use fit formulae for the radioactive energy input,  $\epsilon_{\text{nuc}}$ , and for the average nucleon and proton number,  $\bar{A}$  and  $\bar{Z}$ , that are needed to call the EOS. The expressions that we use in this study

are provided in Appendix A. The energy produced by the *r*-process comes mainly from beta decays (Metzger et al. 2010). Initially, the *r*-process path stays far from stability due to the high neutron densities. During this phase, the neutron separation energy for the nuclei in the *r*-process path is  $S_n \sim 2 - 3$  MeV, which is significantly smaller than the typical beta-decay Q-values around 10 MeV. Fission can be very important in neutron star mergers (Freiburghaus et al. 1999); however it provides significantly less energy than the beta decays (Metzger et al. 2010). Therefore, the energy generation is dominated by beta decays and initially stays approximately constant because the high neutron density and fission cycling maintain the matter at a given path far from stability where all beta decay rates are similar. After the neutrons have run out the *r*-process matter decays to stability and the contribution of beta decays to the energy generation is proportional to  $t^{-\alpha}$  (Metzger et al. 2010; Korobkin et al. 2012). For the phase of constant energy generation we have tried different values of  $\epsilon_{\text{nuc}}$  in post-processing calculations and find that the evolution of temperature does not strongly vary for rates between 2 and 8 MeV nuc $^{-1}$ s $^{-1}$ . In addition, only an upper limit can be determined for the energy that contributes to heat the matter because an unknown part of it escapes in the form of electron antineutrinos.

To account for neutrino energy losses associated with  $\beta$ -decays, we introduce a heating efficiency parameter  $\epsilon_{\text{th}}$  which denotes the fraction of nuclear power which is retained in the matter. Metzger et al. (2010) argue that this fraction must be  $\epsilon_{\text{th}} \approx 0.25 \dots 1$ . Here and in Paper II we adopt a value of  $\epsilon_{\text{th}} = 0.5$ .

While details may benefit from an even more accurate heating treatment, we consider our prescription accurate enough for this first study to explore whether and where heating by radioactive decay makes a noticeable difference with respect to the purely hydrodynamic evolution. We include the heating term explicitly in our energy equation and since the typical heating time-scales are similar to the hydrodynamic time-step, we can use a single time integration scheme for the whole system of equations. This is different from the case where a nuclear network is coupled to the hydrodynamics. The latter case usually requires operator splitting techniques (e.g. Sec. 2 in Rosswog et al. (2009)), since the nuclear and hydrodynamic time-scales can differ by many orders of magnitude.

## 2.4 Heating prescription in previous studies

The rate of nuclear energy generation as a result of *r*-process nucleosynthesis in the ejecta is a crucial input for macronova models. It is directly reflected in the light curves and hence it has a decisive impact on their detectability. Therefore, it is worth briefly comparing the heating rates that have been employed in the different approaches. Tanaka & Hotokezaka (2013) use an energy generation rate that is based on the result of running a nuclear reaction network (Metzger et al. 2010) over the thermodynamic trajectory of a single SPH particle from an early neutron star merger simulation (Rosswog et al. 1999). Since at that time no electron-/positron-captures were included in the models the electron fractions in the ejecta were considered as rather uncertain, although

by now it has turned out that the  $\beta$ -captures only cause minor changes and the ejecta- $Y_e$  stays close to the initial, cold  $\beta$ -equilibrium value. For that reason, (Metzger et al. 2010) adopted an initial value of  $Y_e = 0.1$  to determine the energy generation rate. Barnes & Kasen (2013) used the heating rates from the work of Roberts et al. (2011) where the initial electron fraction of the ejecta was fixed to a value of  $Y_e = 0.2$ . Our calculations (Rosswog et al. 2013; Rosswog 2013), in contrast, start from a realistic cold  $\beta$ -equilibrium and allow for  $Y_e$ -changes due to electron-/positron-captures. We find some trajectories with higher  $Y_e$ , but the large majority is ejected with a very low value of  $Y_e \approx 0.03$ . While all of these values may appear reasonable, it actually turns out that the initial value of the electron fraction does matter and the lower initial electron fraction leads to a lower energy production at late times. To illustrate this, we perform a simple experiment: we take the average trajectory from our reference case, run B, and calculate the energy generation rate once from our best estimate ( $=0.04$ ) and once with an artificially increased value of  $Y_e = 0.2$ . The first is shown as red, and the second one as the dashed green line in Fig. 1. Overall there is reasonably good long-term agreement as can be seen in the left panel. However, after a few days, at the time when the macronovae are expected to peak, the artificially increased  $Y_e$ -case overproduces the heating by a factor of 2–3. As can be seen in Fig. 1, such high  $Y_e$  also results in a less steep decay (with power-law index of 1.2 instead of 1.3). The rate from Tanaka & Hotokezaka (2013), see the blue dotted line, exceeds our heating rate by nearly a factor of 4. These differences will have significant implications on the detectability of the macronovae signals, as we discuss in section 6 of Paper II. For now, we can only speculate that this effect may be due to the less neutron-rich ejecta producing on average lighter radioactive elements with longer half-lives which consequently release their energy later. This question is left for future work.

## 3 IMPACT OF THE HEATING ON THE REMNANT STRUCTURE

To explore the impact that the continuous energy injection has on the remnant morphology we study the evolution of the remnant from a 1.3 and a 1.4  $M_{\odot}$  ns (run B in Tab. 1), once with and once without nuclear energy input (see Fig. 2 left and right column; as explained above, the innermost matter has been cut out and replaced by a point mass). Total nuclear energy which does not escape in the form of neutrinos can be roughly estimated as (cf. Metzger et al. 2010):

$$E_{\text{nuc}} \approx \epsilon_{\text{th}} X_n ((B/A)_r - \Delta_n) \approx 3.6 X_n \text{ MeV nucleon}^{-1}, \quad (3)$$

where  $(B/A)_r \approx 8$  MeV nucleon $^{-1}$  is an approximate average binding energy of the *r*-process nuclei,  $\Delta_n \approx 0.782$  MeV is the Q-value of neutron decay, and  $\epsilon_{\text{th}} = 0.5$  is the adopted value for thermal efficiency (see Sec. 2.2). The quantity  $X_n$  is the initial mass fraction of neutrons, which is determined from nuclear statistical equilibrium (NSE) and turns out to be around  $X_n \approx 0.89$  under typical thermodynamical conditions encountered in the dynamical ejecta.

Table 1 lists more accurate estimates of the total retained

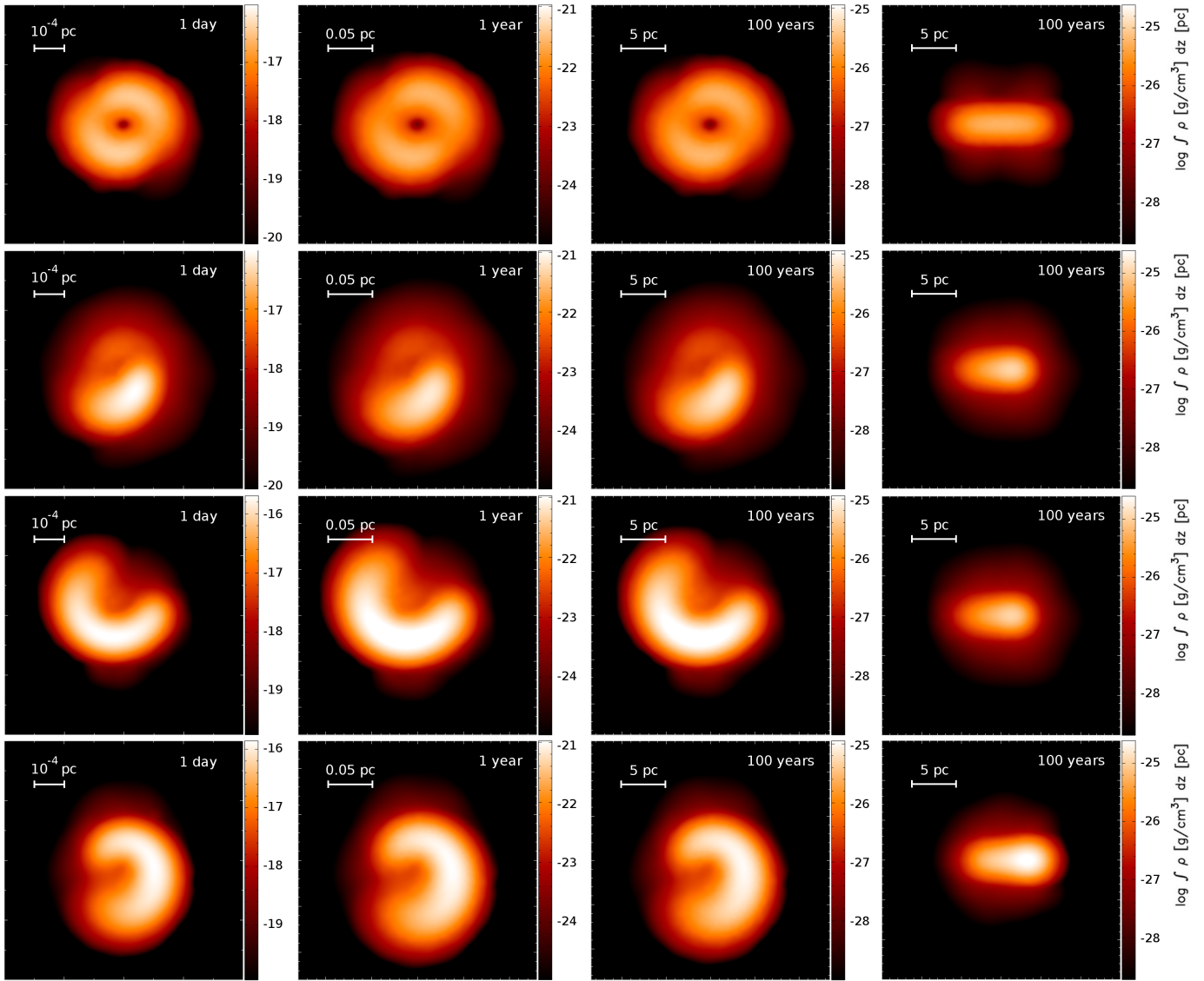


**Figure 6.** Remnant structure at later times. First row:  $2 \times 1.4 M_{\odot}$ , second row:  $1.4$  and  $1.3 M_{\odot}$ , third row:  $1.6$  and  $1.2 M_{\odot}$ , last row:  $1.8$  and  $1.2 M_{\odot}$ . For each case the snapshots show the column densities after 1 d (first column), 1 year (second column) and after 100 years (third column). The fourth column shows the XZ matter distribution at  $t = 100$  years for each case.

nuclear energy  $E_{\text{nuc}}$ , taken directly from the nucleosynthesis network calculations. It is non-negligible in comparison to the kinetic energy and, indeed, the continuous energy injection smoothes out initial inhomogeneities and bloats up the remnant in comparison to the purely adiabatic evolution. We illustrate the density evolution of the ejecta during the first 100 years by taking the SPH particle distributions at the data outputs closest to prescribed times ( $t_0$ : start of longterm evolution, 1 d, 1 month, 100 years) and we show 50 bins of masses and radii in Fig. 3. The average densities drop within years by 36 (40) orders of magnitude with respect to the longterm simulation start (the initial densities inside the neutron stars).

Again for our reference case with  $1.3$  and a  $1.4 M_{\odot}$  ns (run B in Tab. 1), we gauge the impact of the heating on temperature and density evolution. We monitor the maximum and average values of density and temperature, each time with and without heating (see Figs. 4 and 5).

If heating is ignored, both peak (diamond symbol) and average temperatures (dashed line) decrease monotonically due to  $PdV$  work, while the nuclear energy release from radioactive decays leads to a temperature increase up to  $\sim 10^9$  K after about 0.5 s. For  $t \gtrsim 1$  s the temperatures obtained with heating are typically an order of magnitude larger than in the case when heating is ignored. The density evolution for both cases is qualitatively similar, but at any given point in time the density in the heating case is approximately an order of magnitude lower.

Fig. 6 shows snapshots of the remnant column density after 1 d (a typical time for ‘macronovae’ to peak) and also after 1 and 100 years (at these times, depending on the ambient medium density and the exact ejecta properties, see equation (2), the remnant starts becoming decelerated and should produce radio flares). All remnants expand in a nearly perfectly homologous manner. In the symmetric case ( $2 \times 1.4 M_{\odot}$ ) matter is ‘donut-shaped’ after one day



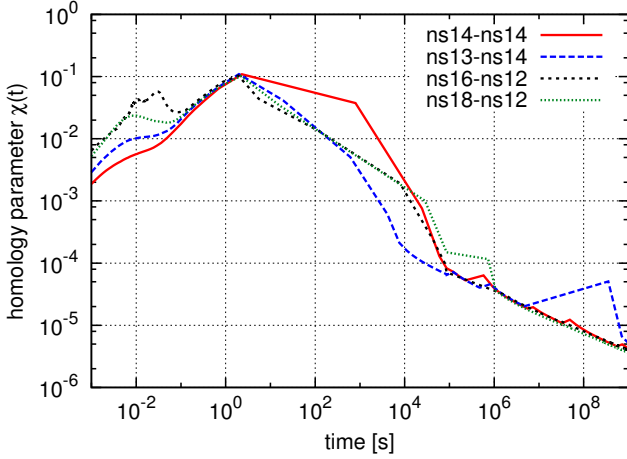


**Figure 7.** Time evolution of the homology parameter, defined as the relative change of velocity due to dynamic acceleration:  $\chi(t) \equiv \frac{\bar{a}t}{\bar{v}}$ . Distributions become homologous up to 1 per cent after about 100 s for all non-equal mass cases, and after about 2000 s for the symmetric case of 1.4-1.4  $M_{\odot}$ .

and keeps expanding self-similarly up to 100 years, when it reaches a radius of  $r_{\text{cyl}} \sim 8$  pc and a height  $z \sim 3$  pc. In other words sphericity has not been reached and the remnant still clearly remembers the original orbital plane. So 100 years after the merger the remnant still carries the imprint of the initial binary mass ratio, equal (two-armed spiral) and unequal mass systems (one-armed spiral) can still be clearly distinguished.

To quantify the deviations from a perfectly homologous evolution we introduce a homology parameter

$$\chi(t) \equiv \bar{a}t/\bar{v} \quad (4)$$

with  $\bar{v}$  and  $\bar{a}$  being the average velocity and acceleration. In the case of perfectly homologous expansion, this parameter should be equal to zero. Fig. 7 depicts the evolution of  $\chi(t)$  for the considered cases. After an initial increase,  $\chi(t)$  reaches a maximum at  $t \sim 1$  s, the time when the ejecta have maximal acceleration due to the radioactive heating. After  $t = 100$  s the unequal mass cases are homologous to better than 1 per cent, while the equal-mass case of 1.4–1.4  $M_{\odot}$  reaches the same degree only after about 2000 s. At the times that are relevant for our macronova calculations ( $\sim 1$  d), the expansion is homologous to 0.01 per cent in all cases.

## 4 NUCLEOSYNTHESIS

### 4.1 How accurate are nucleosynthesis calculations with post-processed temperatures?

It is of particular interest to see whether a consistent accounting for the heating in the hydrodynamics is crucial for the final *r*-process abundance distribution. So far, starting with Freiburghaus et al. (1999) most existing studies have simply post-processed existing trajectories with nuclear networks to estimate temperatures, thereby implicitly assuming that the accelerated expansion due to the nuclear heating is negligible. A notable exception is the study by Goriely et al.

(2011b), which has studied the effect by means of a one-zone dynamical model with nuclear heating feedback on the density, therefore accounting for an additional expansion. However, in their model the observed effect on the density evolution was very small. By inspecting randomly chosen trajectories from our reference run B (with/without heating), we find that the post-processed temperatures are actually rather accurate. In Fig. 8, left panel, we compare the different temperature evolutions for the case of an exemplary particle trajectory: once with heating ignored and temperature evolution determined entirely by adiabatic expansion (dashed, blue, ‘hydro, heating ignored’), once with the temperature directly taken from the hydrodynamic evolution including heating (as detailed in Appendix A; solid, red, ‘hydro + nuclear heating’) and once as reconstructed by running a nuclear network over a purely hydrodynamic trajectory (as detailed in Freiburghaus et al. (1999); solid, green, ‘temperature from post-processing’). This post-processed temperature actually agrees closely with the one found when heating is accounted for properly. Since the additional expansion due to the radioactive heating is ignored, the post-processing approach slightly overestimates the temperatures. Given that the nuclear energy release has a substantial impact on the long-term matter evolution, see below, it is not self-evident that abundances can be reliably calculated in this ad hoc manner. Nevertheless, it turns out that the final abundance patterns closely agree with each other (see Fig. 8).

### 4.2 Dynamic ejecta versus neutrino-driven winds

We had recently explored the nucleosynthesis inside the dynamic ejecta of compact binary mergers (Korobkin et al. 2012) and found that all of the ejecta matter undergoes a very robust, ‘strong’ *r*-process (also confirmed in Bauswein et al. 2013). The abundance patterns showed some sensitivity to the nuclear physics input, but are essentially independent of the parameters of the binary system: all coalescences produced practically identical abundance patterns beyond  $A = 130$ , it does not even matter whether a nsns or a nsbh system is merging.

But as pointed out above, compact binary mergers also eject matter via different channels. With neutrino luminosities of  $\sim 10^{53}$  erg/s, neutron star merger remnants drive strong baryonic winds (Ruffert et al. 1997; Rosswog & Ramirez-Ruiz 2002, 2003; Rosswog et al. 2003; Dessart et al. 2009), similar to new-born neutron stars (Duncan et al. 1986; Qian & Woosley 1996). This is an additional mass-loss channel and it can very plausibly complement the heavy element nucleosynthesis and produce additional electromagnetic transients.

The total amount of mass that is ejected by such winds is not trivial to estimate. Dessart et al. (2009) find overall mass-loss rates of  $\dot{M}^{\text{wind}} \sim 10^{-3} M_{\odot}/\text{s}$ . Once the central object collapses to a black hole this rate is expected to drop abruptly since a substantial part of the neutrino emission comes from its surface layers. For an assumed collapse after 100 ms Dessart et al. (2009) estimate  $< 10^{-4} M_{\odot}$  to be ejected by winds. This number, however, is rather uncertain and could be easily substantially larger for a number of reasons. First, the time scale for the collapse is not well known and with recent estimates of the minimum, cold neu-

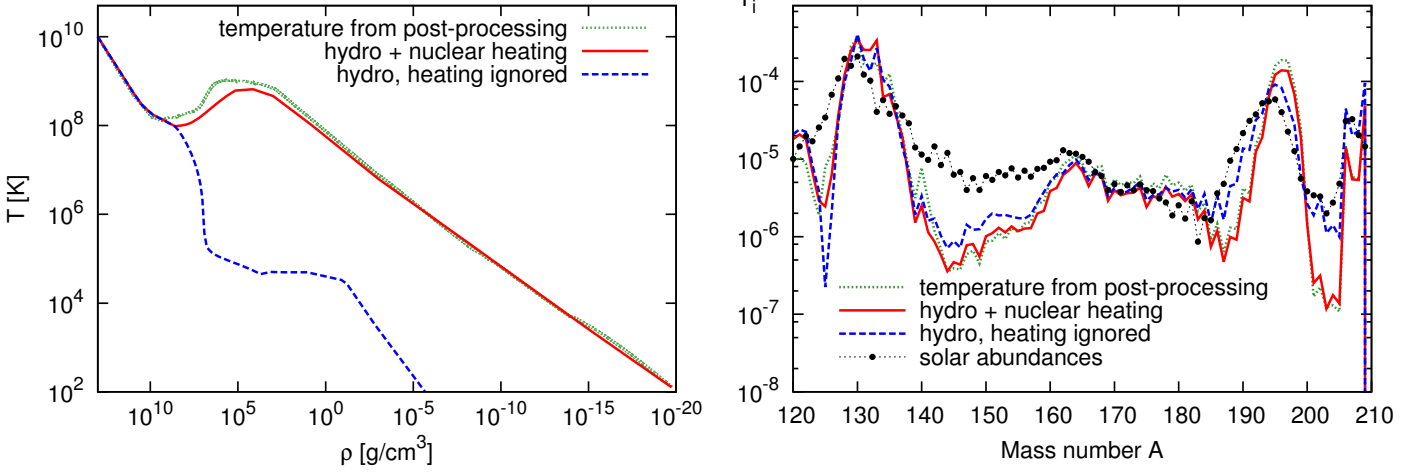


**Figure 8.** Assessing the quality of post-processed temperatures. To illustrate the quality of the post-processing approximation (assume density evolution as given) obtain the temperature from the entropy production due to nuclear reactions) we compare it for a randomly chosen trajectory with the corresponding trajectory whose temperature comes from evolving hydrodynamics and nuclear heating concordantly. The blue line labels the ‘hydrodynamic’ temperatures when heating is ignored, and the red line is the result from the ‘hydrodynamics + nuclear heating’ calculations. The post-processed temperature is overlaid as the green line. Overall, the agreement is remarkably good. The resulting abundances are also in close agreement (‘hydrodynamics + nuclear heating’ in red, ‘post-processed’ in green).

tron star mass around  $2.0 M_{\odot}$  (Antoniadis & et al. 2013) the differentially rotating central core with temperatures in excess of 10 MeV could be stable for much longer. In fact, it is entirely plausible that the low mass end of the neutron star binary population could produce a very massive neutron star as final product rather than a black hole. The wind would then have a substantially longer duration, comparable to the Kelvin-Helmholtz time scale of many seconds. For such cases, however, it remains an open question whether/how baryonic pollution could be avoided and a (short) GRB could be launched. Secondly, neutron stars are endowed by possibly strong initial magnetic fields and the dynamics during a merger offers ample opportunities to amplify these initial seeds (Price & Rosswog 2006; Liu et al. 2008; Anderson et al. 2008; Rezzolla et al. 2011; Giacomazzo et al. 2011; Zrake & MacFadyen 2013) to substantial fractions of the equipartition strength. A merger remnant rotating at  $\sim 1$  ms with a strong magnetic field ( $\sim 10^{16}$  G) could easily increase the amount of launched mass by orders of magnitude (Thompson 2003). For these reasons, we parametrize the mass in these winds in a range from  $10^{-4}$  to  $10^{-2} M_{\odot}$ .

In the following we apply a very simple wind model. It is meant to illustrate basic features of the nucleosynthesis and to discuss the plausibility of a second radioactively powered transient beside the usual ‘macronovae’ from the dynamic ejecta (see Paper II). This topic deserves more work beyond our simple model, ideally with multi-dimensional neutrino-hydrodynamic simulations.

In our simple approach we calculate the bulk properties of  $\nu$ -driven winds by means of the estimates from Qian & Woosley (1996). The asymptotic value of the wind electron fraction can be estimated as

$$Y_e^{\text{fin,wind}} \approx \left( 1 + \frac{L_{\bar{\nu}_e} \epsilon_{\bar{\nu}_e} - 2\Delta + 1.2\Delta^2/\epsilon_{\bar{\nu}_e}}{L_{\nu_e} \epsilon_{\nu_e} + 2\Delta + 1.2\Delta^2/\epsilon_{\nu_e}} \right)^{-1}, \quad (5)$$

where  $L_{\nu_e}/L_{\bar{\nu}_e}$  are the luminosities of electron neutrinos and anti-neutrinos,  $\epsilon = \langle E^2 \rangle / \langle E \rangle$ ,  $E$  being the neutrino energy, and  $\Delta$  the neutron-proton mass energy difference of 1.293 MeV. To estimate  $\epsilon$  we simply multiply our values for  $\langle E \rangle$  by a factor of 1.3, as appropriate for Maxwell-Boltzmann distributions. If the neutrino properties from the simulations are inserted (see Table 1), one finds values between  $Y_e^{\text{fin,wind}} = 0.28$  and 0.40. Interestingly, the asymptotic electron fraction increases with decreasing mass ratio, so that the symmetric system produces the lowest  $Y_e$  values. Again based on Qian et al. (1997), we find that the average entropies in the wind are very close to  $8 k_B$  per baryon for all our cases.

In our simple model, we produce a synthetic trajectory with a linear expansion profile  $\rho(t) = \rho_0(1 + vt/R_0)^{-3}$ , starting from the entropy  $s_0 = 8 k_B/\text{baryon}$  and a range of electron fractions, corresponding to the runs A-D. Based on the results of Dessart et al. (2009), their fig. 2, we select the initial density  $\rho_0 = 5 \times 10^7 \text{ g cm}^{-3}$  and the characteristic radius  $R_0 = 200$  km in a way that temperature is safely above the NSE threshold. We then run the nucleosynthesis network, using the calculated values of  $\rho(t)$  and self-consistently incrementing the entropy in the same way as described above for the dynamical ejecta case. The temperature of the trajectory at every time is calculated using the Helmholtz EOS and the needed values of  $\bar{A}$  and  $\bar{Z}$  are computed from the network. For the expansion velocity, we use the escape velocity from the launch region ( $v = 0.11c$ ).

We find element distributions between  $A = 50$  and 130 in a weak r-process. In Fig. 9 we show the resulting nucleosynthesis for all four runs and each time we distinguish between the dynamic ejecta (blue) and the  $\nu$ -wind (red). Note that this shows the individual compositions for these two types of ejecta, not considering how much ejecta mass is involved in each of them. As pointed out by Korobkin et al. (2012), the dynamic ejecta abundances for  $A \gtrsim 130$  hardly vary

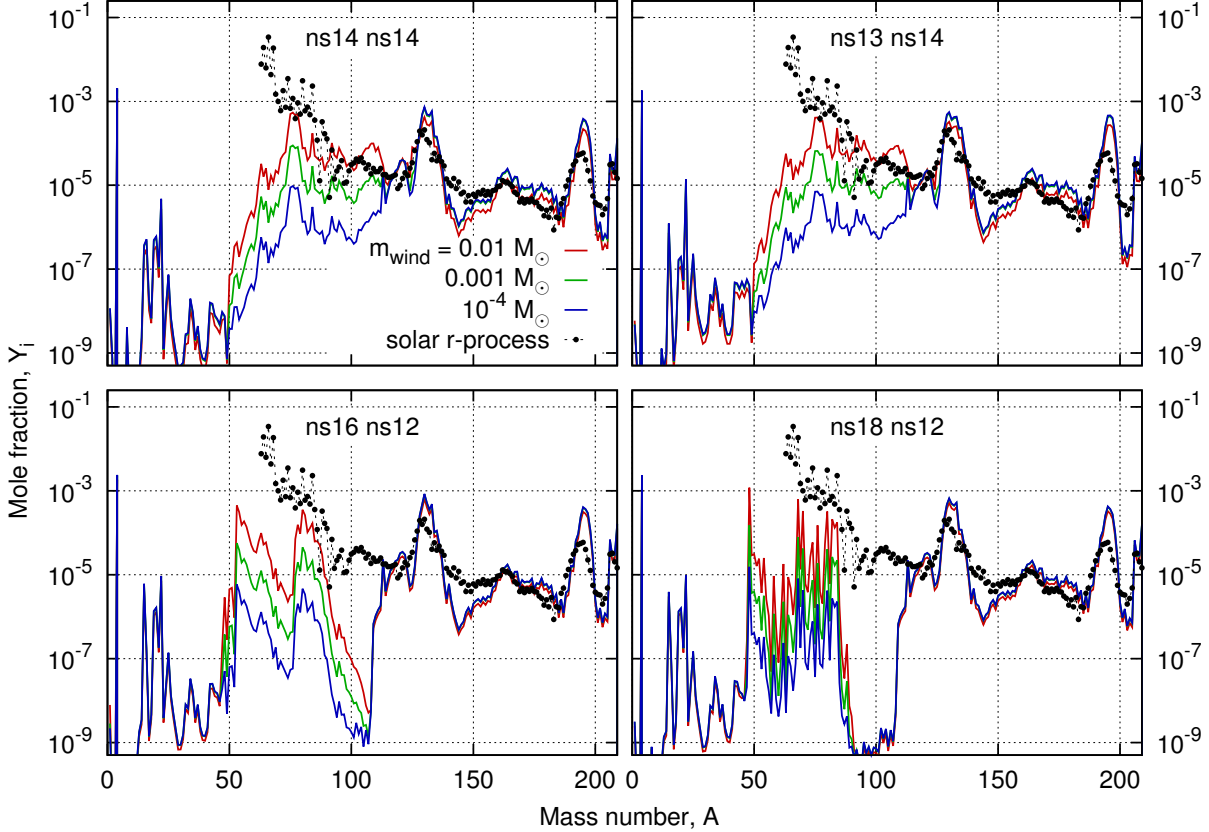


**Figure 10.** Resulting abundances from the sum of the dynamic ejecta and the neutrino-driven winds for all four models. For the dynamic ejecta we use the masses ( $m_{\text{ej}}$ ) as found in the simulations, see Tab. 1, for the neutrino-driven winds the masses are poorly known and therefore parametrized from  $m_{\text{wind}} = 10^{-4} \dots 10^{-2} M_{\odot}$ . Note that the abundance pattern of the wind component varies substantially between different runs, while it hardly varies for the dynamic ejecta component ( $A \gtrsim 110$ ).

at all from case to case. The  $\nu$ -wind abundances, in contrast, produce matter in the range from  $A = 50$  to 130 with substantial variations between different merger cases. The latter is due to the sensitivity of the nucleosynthesis to  $Y_e$ , which, in turn, is set by the neutrino properties. In Fig. 10 we show the abundances for both wind and dynamic ejecta. We use the simulation results for the masses of the dynamic ejecta and  $10^{-4}$ ,  $10^{-3}$  and  $10^{-2} M_{\odot}$  for the masses in the wind. The differences in the abundances below the second peak will naturally lead to variations in the relative abundances between heavy *r*-process elements and elements with  $A < 130$ , and this is important to understand the role of neutron star mergers in the chemical history of our galaxy. We also note that the neutrino-driven winds produce a range of radioactive isotopes (though no  $^{56}\text{Ni}$ ) that are long-lived enough to still be present when the wind matter becomes transparent, i.e. one can expect a second, radioactively powered transient. Its details are discussed in Sec. 5 of Paper II. It turns out that our simple neutrino-driven wind model produces an electromagnetic transient that is more promising for coincident detection with a GW signal than the ‘macronova’ signal from the dynamic ejecta, mainly due to the different opacities (Kasliwal & Nissanke 2013).

## 5 SUMMARY AND DISCUSSION

In this work we have focused on the long-term evolution of the dynamic ejecta of a neutron star merger and in particular on the role that the freshly synthesized and radioactively decaying *r*-process elements play. We have included the energetic feedback from radioactive decays based on nuclear network calculations into the hydrodynamic evolution. Contrary to existing simulations which typically stop after  $\sim 20$  ms, we follow the ejecta evolution through all phases where electromagnetic emission is expected to occur and we only stop the simulations after 100 years. At this time (at latest) the ejecta should have swept up ambient matter comparable to their own mass and start becoming decelerated, a process that is not modelled here. These simulations allow us to accurately quantify how homologous the expansion actually is. We find that in all cases the degree of homology after  $10^4$  s is better than 0.1 per cent (see Fig. 7).

We find that the radioactive heating has a substantial impact on the morphology and efficiently smoothes out initial inhomogeneities. Although the nuclear energy input does alter dynamics and morphology it does not erase the memory of the initial binary system parameters. For example, the remnant matter keeps its ‘donut shape’ in the case of a perfectly symmetric ( $q = 1$ ) merger until at least 100 years

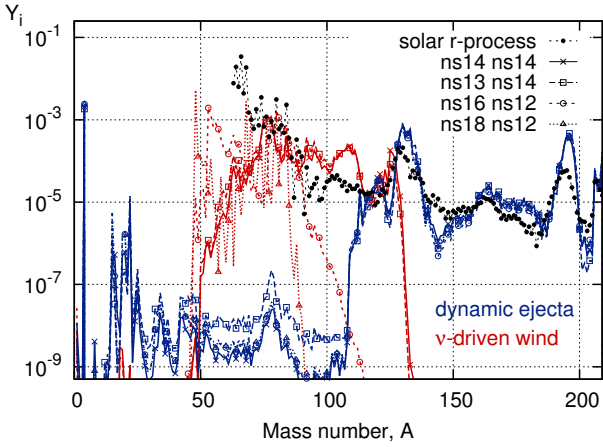


**Figure 9.** Robustness versus variability in the abundance patterns: final abundances from both the dynamic ejecta (blue) and the neutrino-driven wind (red) for our four simulations (each of the abundance curves is normalized separately,  $\sum_i A_i Y_i = 1$ ). The numbers in the legend indicate the neutron star masses in units of  $0.1 M_\odot$ , i.e. ns13 ns14 refers to a system with a 1.3 and a  $1.4 M_\odot$  neutron star. Note that dynamic ejecta produce an extremely robust abundance pattern for  $A > 110$ , while the patterns in neutrino-driven winds vary strongly between different merger events.

after the coalescence, while asymmetric mergers still carry the imprint of their initial mass ratio.

A number of recent studies [Panov et al. (2008), Goriely, Bauswein & Janka (2011a), Goriely et al. (2011b); Roberts et al. (2011); Korobkin et al. (2012); Bauswein et al. (2013)] have dealt with the dynamic ejecta of neutron star mergers. Most studies have simply post-processed the temperature along trajectories of prescribed density, thereby ignoring the effect of the radioactive heating on the density evolution. Only Goriely et al. (2011b) have investigated this effect by means of a one-zone expansion model. None of the studies that we are aware of has included the energetic feedback from nuclear reactions in a 3D hydrodynamic simulation. But despite the large impact in the long-run, we find that such post-processed nucleosynthesis results agree actually well with those calculated including nuclear heating. This is mainly because in the early stages where the r-process takes place (seconds), the impact of the energy release on the density evolution is still small.

While each of the above mentioned studies had their specific focus and contribution, they all agree with the basic picture outlined in Freiburghaus et al. (1999): the dynamic ejecta seem to naturally produce the ‘strong’ r-process component and the ejected amounts of matter are consistent with contributing a major part to the overall galactic r-process inventory. The resulting abundance pattern is essentially independent of the exact system that merges (Korobkin et al. 2012), i.e. it hardly matters whether two neutron stars of different masses or even a neutron star black hole system merges. All these events produce essentially identical abundance signatures above  $A \gtrsim 130$ , this is illustrated for runs A-D in Fig. 9 (blue curves).

For two reasons we consider the conclusion that the dynamic ejecta are excellent candidates for the ‘strong’ r-process as

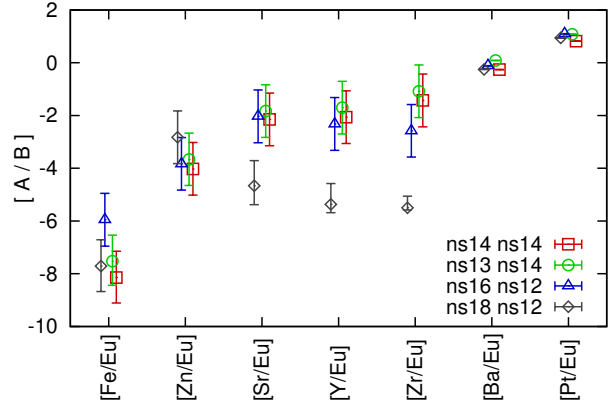


**Figure 11.** Abundance ratios of representative elements with respect to Eu for the sum of dynamic ejecta and neutrino-driven winds. The error bars reflect the estimated uncertainty in the mass ejected in neutrino-driven winds, which is varied from  $10^{-4} M_\odot$  and  $10^{-2} M_\odot$ . Ba and Pt represent strong r-process components and exhibit very little scatter with respect to both the merging system, and the unknown mass of the wind component. Sr, Y and Zr are the weak r-process elements, which are very sensitive to the merging system, in particular the electron fraction. Fe and Zn represent the iron group elements; they are under-produced for all combinations of masses and merging systems.

very robust. First, the ejecta amounts found by different groups are not identical, but given the large uncertainties in the merger rates all of them are consistent with being an important r-process source. For nsns mergers we found a range from  $8 \times 10^{-3} - 4 \times 10^{-2} M_\odot$  (Rosswog 2013), approximate GR calculations find  $10^{-3} - 2 \times 10^{-2} M_\odot$  (Bauswein et al. 2013) and full GR calculations (Hotokezaka et al. 2013) find  $10^{-4} - 10^{-2} M_\odot$ . Even the results for our Newtonian nsbh calculations agree quite well with the GR results [see Tab. 1 in (Rosswog 2013) and Kyutoku et al. (2013)]. Secondly, the robustness of the abundance pattern is due to the extreme neutron-richness of the ejecta, we find typical values of  $Y_e \approx 0.03$  (Korobkin et al. 2012; Rosswog et al. 2013). This value is determined by the cold  $\beta$ -equilibrium in the initial neutron star and it could change for stars of different compactness (say, due to a different EOS or a different treatment of gravity). But in this range even  $Y_e$ -variations by factors of a few hardly change the resulting abundance pattern. Only at values beyond  $Y_e \approx 0.18$  does the pattern of the heaviest elements ( $A \gtrsim 130$ ) become sensitive to the exact value of  $Y_e$  (see fig. 8 in Korobkin et al. (2012)). This makes compact binary mergers natural candidates for the sources of the robust, ‘strong’ r-process component. Whether neutron star mergers can also produce the earliest enrichments of galaxies with r-process elements remains to be further investigated, though.

We have also briefly investigated the nucleosynthesis in the neutrino-driven winds from a neutron star merger remnant. The nucleosynthesis therein is mainly determined by the asymptotic electron fraction  $Y_e$ , which, in turn, is set by the neutrino properties. These winds produce a weak r-process with elements from  $A = 50$  to 130 and the abundance patterns vary substantially between different merging systems.

We stress once more that the model discussed here is very simple, but it indicates that this topic is worth more detailed neutrino-hydrodynamics studies.

Observations of low-metallicity stars give an indication that the *r*-process elements related to the production of the heaviest elements (an indicator is the *r*-process element Eu) are not correlated with the Fe-group, i.e. Fe is not co-produced in events responsible for the Eu production, or provides at most a minor contribution (Cowan et al. 2005). Intermediate-heavy elements like Sr, Y, Zr (also called LEPP elements) show a weak correlation (Cowan et al. 2005), i.e. can be co-produced, but probably have their dominant contribution from a different process ( $\nu$ -p process, weak *r*-process, charged particle process, see e.g. Qian & Wasserburg (2007, 2008)). The co-production with Eu for those stars most strongly enriched in this heavy *r*-process element, seems to give a contribution of about 5–10 per cent to the total Sr, Y, Zr and Ag production (see fig. 1 in Montes et al. (2007)). On the other hand, Ba, La, Ce, Nd and Sm, as signatures of a strong *r*-process, are all co-produced in their solar *r*-process contribution.

If neutron star mergers are the source of this heavy element *r*-process, we expect a similar behaviour in their ejecta. Fig. 11 gives an indication of exactly this behaviour with a Ba/Eu ratio equaling the solar *r*-process pattern, while Sr, Y, Zr ratios are down by a factor of 10-100, and the Fe-group shows a negligible contribution. Note that in (total) solar abundances Ba is dominated by the *s*-process. This explains the difference between [Ba/Eu] and [Pt/Eu] in Fig. 11, which in dynamic merger ejecta are produced in their solar ‘*r*-process contribution’ (see Fig. 10). Thus, even for the highest possible contribution of wind ejecta, weak or strong correlations are not destroyed and neutron star mergers provide exactly the behaviour required from the strong *r*-process source.

## ACKNOWLEDGEMENTS

We would like to thank C. Winteler for providing his nucleosynthesis network code and for his continued support. This work has also benefited from the stimulating discussions at the MICRA workshop in 2013. This work was supported by DFG grant RO-3399, AOBJ-584282 and by the Swedish Research Council (VR) under grant 621-2012-4870. The simulations of this paper were performed on the facilities of the Höchstleistungsrechenzentrum Nord (HLRN). A.A. is supported by the Helmholtz-University Young Investigator grant No. VH-NG-825. F.-K. T. gratefully acknowledges support from the Swiss National Science Foundation (SNF), both S.R. and F.-K. T. have been supported by Compstar. A.A. and F.-K. T. are part of Collaborative Research Program Eurogenesis/MASCHE funded by the European Science Foundation. T.P. is supported by an ERC advanced grant (GRBs) and by the I-CORE Program of the Planning and Budgeting Committee and The Israel Science Foundation (grant No 1829/12).

## REFERENCES

- Abadie J. et al. 2010, CQG, 27, 173001, ADS  
 Abbott B. P. et al. 2009, Rep. Progress Phys., 72, 076901, ADS  
 Anderson M., Hirschmann E. W., Lehner L., Liebbling S. L., Motl P. M., Neilsen D., Palenzuela C., Tohline J. E., 2008, PRL, 100, 191101, ADS  
 Antoniadis J., et al. 2013, Science, 340, 448, ADS  
 Arcones A., Janka H.-T., Scheck L., 2007, A&A, 467, 1227, ADS  
 Barnes J., Kasen D., 2013, ApJ, 775, 18, ADS  
 Bauswein A., Goriely S., Janka H.-T., 2013, ApJ, 773, 78, ADS  
 Beloborodov A. M., 2008, in M. Axelsson ed., AIPConf. Ser. Vol. 1054, Hyper-accreting Black Holes. pp 51–70, ADS  
 Bloom J. S., Kulkarni S. R., Djorgovski S. G., 2002, AJ, 123, 1111, ADS  
 Caballero O. L., McLaughlin G. C., Surman R., 2012, ApJ, 745, 170, ADS  
 Cowan J. J. et al. 2005, ApJ, 627, 238, ADS  
 Cutler C., Flanagan É. E., 1994, Phys. Rev. D, 49, 2658, ADS  
 Dessart L., Ott C. D., Burrows A., Rosswog S., Livne E., 2009, ApJ, 690, 1681, ADS  
 Duncan R. C., Shapiro S. L., Wasserman I., 1986, ApJ, 309, 141, ADS  
 Eichler D., Livio M., Piran T., Schramm D. N., 1989, Nature, 340, 126, ADS  
 Fernández R., Metzger B. D., 2013, MNRAS, 435, 502, ADS  
 Fischer T., Whitehouse S. C., Mezzacappa A., Thielemann F.-K., Liebendörfer M., 2010, A&A, 517, A80, ADS  
 Fong W., Berger E., Fox D. B., 2010, ApJ, 708, 9, ADS  
 Freiburghaus C., Rosswog S., Thielemann F.-K., 1999, ApJ, 525, L121, ADS  
 Fryer C. L., Woosley S. E., Hartmann D. H., 1999, ApJ, 526, 152, ADS  
 Giacomazzo B., Rezzolla L., Baiotti L., 2011, Phys. Rev. D, 83, 044014, ADS  
 Goriely S., Bauswein A., Janka H.-T., 2011, ApJL, 738, L32, ADS  
 Goriely S., Chamel N., Janka H.-T., Pearson J. M., 2011, A&A, 531, A78, ADS  
 Grossman D., Korobkin O., Rosswog S., Piran T., 2013, preprint (arXiv:1307.2943)  
 Hotokezaka K., Kiuchi K., Kyutoku K., Okawa H., Sekiguchi Y.-i., Shibata M., Taniguchi K., 2013, Phys. Rev. D, 87, 024001, ADS  
 Hüdepohl L., Müller B., Janka H.-T., Marek A., Raffelt G. G., 2010, PRL, 104, 251101, ADS  
 Kasen D., Badnell N. R., Barnes J., 2013, ApJ, 774, 25, preprint (arXiv:1303.5788)  
 Kasliwal M. M., Nissanke S., 2013, preprint (arXiv:1309.1554)  
 Kelley L. Z., Mandel I., Ramirez-Ruiz E., 2012, Phys. Rev. D, 87, 17, ADS  
 Korobkin O., Rosswog S., Arcones A., Winteler C., 2012, MNRAS, 426, 1940, ADS  
 Kulkarni S. R., 2005, preprint (arXiv:astro-ph/0510256)  
 Kyutoku K., Ioka K., Shibata M., 2013, Phys. Rev. D, 88,

- 041503, ADS  
Lattimer J. M., Mackie F., Ravenhall D. G., Schramm D. N., 1977, *ApJ*, 213, 225, ADS  
Lattimer J. M., Schramm D. N., 1974, *ApJ*, 192, L145, ADS  
Lee W. H., Ramirez-Ruiz E., 2007, *New Journal of Physics*, 9, 17, ADS  
Lee W. H., Ramirez-Ruiz E., López-Cámara D., 2009, *ApJL*, 699, L93, ADS  
Li L., Paczyński B., 1998, *ApJL*, 507, L59, ADS  
Liu Y. T., Shapiro S. L., Etienne Z. B., Taniguchi K., 2008, *Phys. Rev. D*, 78, 024012, ADS  
Maggiore M., 2007, *Gravitational Waves. Vol. 1*, Oxford University Press, ISBN:978-0-19-857074-5  
Malkus A., Kneller J. P., McLaughlin G. C., Surman R., 2012, *Phys. Rev. D*, 86, 085015, ADS  
Metzger B. D., Arcones A., Quataert E., Martinez-Pinedo G., 2010, *MNRAS*, 402, 2771, ADS  
Metzger B. D., Berger E., 2012, *ApJ*, 746, 48, ADS  
Metzger B. D. et al. 2010, *MNRAS*, 406, 2650, ADS  
Metzger B. D., Piro A. L., Quataert E., 2008, *MNRAS*, 390, 781, ADS  
Metzger B. D., Piro A. L., Quataert E., 2009, *MNRAS*, 396, 304, ADS  
Monaghan J. J., 2005, *Rep. Progress Phys.*, 68, 1703, ADS  
Montes F. et al. 2007, *ApJ*, 671, 1685, ADS  
Nakar E., 2007, *Phys. Rep.*, 442, 166, ADS  
Nakar E., Piran T., 2011, *Nature*, 478, 82, ADS  
Narayan R., Paczyński B., Piran T., 1992, *ApJ*, 395, L83, ADS  
Narayan R., Piran T., Shemi A., 1991, *ApJ*, 379, L17, ADS  
Nissanke S., Kasliwal M., Georgieva A., 2013, *ApJ*, 767, 124, ADS  
Panov I. V., Korneev I. Y., Thielemann F.-K., 2008, *Astronomy Letters*, 34, 189, ADS  
Piran T., 2004, *Rev. Modern Phys.*, 76, 1143, ADS  
Piran T., Nakar E., Rosswog S., 2013, *MNRAS*, 430, 2121, ADS  
Price D. J., Rosswog S., 2006, *Science*, 312, 719, ADS  
Qian Y.-Z., Haxton W. C., Langanke K., Vogel P., 1997, *Phys. Rev. C*, 55, 1532, ADS  
Qian Y.-Z., Wasserburg G. J., 2007, *Phys. Rep.*, 442, 237, ADS  
Qian Y.-Z., Wasserburg G. J., 2008, *ApJ*, 687, 272, ADS  
Qian Y.-Z., Woosley S. E., 1996, *ApJ*, 471, 331, ADS  
Rezzolla L., Giacomazzo B., Baiotti L., Granot J., Kouveliotou C., Aloy M. A., 2011, *ApJ*, 732, L6, ADS  
Roberts L. F., Kasen D., Lee W. H., Ramirez-Ruiz E., 2011, *ApJL*, 736, L21+, ADS  
Roberts L. F., Woosley S. E., Hoffman R. D., 2010, *ApJ*, 722, 954, ADS  
Rosswog S., 2005, *ApJ*, 634, 1202, ADS  
Rosswog S., 2009, *New Astron. Rev.*, 53, 78, ADS  
Rosswog S., 2013, *R. Soc. Lond. Philos. Trans. Ser. A*, 371, 20272, ADS  
Rosswog S., Davies M. B., 2002, *MNRAS*, 334, 481, ADS  
Rosswog S., Davies M. B., Thielemann F.-K., Piran T., 2000, *A&A*, 360, 171, ADS  
Rosswog S., Liebendörfer M., 2003, *MNRAS*, 342, 673, ADS  
Rosswog S., Liebendörfer M., Thielemann F.-K., Davies M. B., Benz W., Piran T., 1999, *A&A*, 341, 499, ADS  
Rosswog S., Piran T., Nakar E., 2013, *MNRAS*, 430, 2585, ADS  
Rosswog S., Price D., 2007, *MNRAS*, 379, 915, ADS  
Rosswog S., Ramirez-Ruiz E., 2002, *MNRAS*, 336, L7, ADS  
Rosswog S., Ramirez-Ruiz E., 2003, *MNRAS*, 343, L36, ADS  
Rosswog S., Ramirez-Ruiz E., Davies M. B., 2003, *MNRAS*, 345, 1077, ADS  
Rosswog S., Ramirez-Ruiz E., Hix W. R., 2009, *ApJ*, 695, 404, ADS  
Rosswog S., Ramirez-Ruiz E., Hix W. R., Dan M., 2008, *Computer Physics Communications*, 179, 184, ADS  
Ruffert M., Janka H., Takahashi K., Schaefer G., 1997, *A & A*, 319, 122, ADS  
Sengupta A. S., the Ligo Scientific Collaboration the Virgo Collaboration 2010, *Journal of Physics Conference Series*, 228, 012002, ADS  
Shen H., Toki H., Oyamatsu K., Sumiyoshi K., 1998a, *Nuclear Physics A*, 637, 435, ADS  
Shen H., Toki H., Oyamatsu K., Sumiyoshi K., 1998b, *PTP*, 100, 1013, ADS  
Smith J. R., 2009, *CQG*, 26, 114013, ADS  
Snedden C., Cowan J. J., Gallino R., 2008, *ARA&A*, 46, 241, ADS  
Springel V., 2010, *ARAA*, 48, 391, ADS  
Surman R., McLaughlin G. C., Ruffert M., Janka H., Hix W. R., 2008, *ApJL*, 679, L117, ADS  
Tanaka M., Hotokezaka K., 2013, *ApJ*, 775, 113, ADS  
Thielemann F.-K. et al. 2011, *Progress Part. Nucl. Phys.*, 66, 346, ADS  
Thompson T. A., 2003, *ApJL*, 585, L33, ADS  
Timmes F. X., Swesty F. D., 2000, *ApJS*, 126, 501, ADS  
Wanajo S., Janka H.-T., 2012, *ApJ*, 746, 180, ADS  
Winteler C., 2012, PhD thesis, University Basel, CH, ADS  
Winteler C., Käppeli R., Perego A., Arcones A., Vasset N., Nishimura N., Liebendörfer M., Thielemann F.-K., 2012, *ApJL*, 750, L22, ADS  
Zrake J., MacFadyen A. I., 2013, *ApJ*, 769, L29, ADS

This paper has been typeset from a  $\text{\TeX}/\text{\LaTeX}$  file prepared by the author.

## APPENDIX A: FIT FORMULAE FOR THE HEATING DUE TO NUCLEAR REACTIONS

The call of the Helmholtz equation of state requires

$$\bar{A} = \left( \sum_i \frac{X_i}{A_i} \right)^{-1} \quad (\text{A1})$$

$$\bar{Z} = \bar{A} \sum_i Y_i Z_i \quad (\text{A2})$$

on input, where the index runs over all nuclear species including neutrons and protons. From our study (Korobkin et al. 2012) we have deduced the following fit formulae:

$$\bar{A}(t) = \begin{cases} A_0 + A_1(t_0 - t)^{\alpha_1} & t \leq t_0 \\ A_\infty + A_2(t - t_1)^{\alpha_2} + C_1 e^{-\frac{t}{\tau_1}} + C_2 e^{-\frac{t}{\tau_2}} & t > t_0 \end{cases} \quad (\text{A3})$$

$$\bar{Z}(t) = \begin{cases} Z_0 + B_1(t_0 - t)^{\beta_1} & t \leq t_0 \\ Z_\infty + B_2 t^{\beta_2} + B_3 t^{\beta_3} & t > t_0 \end{cases} \quad (\text{A4})$$

and

$$\dot{\epsilon}(t) = 2 \times 10^{18} \frac{\text{erg}}{\text{g} \cdot \text{s}} \left( \frac{1}{2} - \frac{1}{\pi} \arctan \frac{t - 1.3 \text{ s}}{0.11 \text{ s}} \right)^{1.3} \times \left( \frac{\epsilon_{th}}{0.5} \right) \quad (\text{A5})$$

with the fit parameters having the following values:  $t_0 = 1.07$  s,  $t_1 = 0.4$  s,  $\tau_1 = 7.83 \times 10^8$  s,  $\tau_2 = 1.12 \times 10^5$  s,  $A_0 = 0.69$ ,  $A_1 = 0.4922$ ,  $\alpha_1 = -1.328$ ,  $A_\infty = 149.5000$ ,  $A_2 = 16.7200$ ,  $\alpha_2 = -1.9100$ ,  $C_1 = 2.1370$ ,  $C_2 = 0.6838$ ,  $Z_0 = -0.2100$ ,  $B_1 = 0.2783$ ,  $\beta_1 = -1.5373$ ,  $Z_\infty = 61.2000$ ,  $B_2 = -3.0000$ ,  $\beta_2 = -0.1500$ ,  $B_3 = 8.8650$ ,  $\beta_3 = -3.7970$ .